Fabrication and characterization of polyvinylidene fluoride/zinc oxide membranes with antibacterial property

Juan Xiong, Yexia Gong, Cong Ma, Xingtao Zuo and Jiajie He

ABSTRACT

The hydrophilic and antimicrobial polyvinylidene fluoride (PVDF) membrane was fabricated by phase inversion method. The prepared membranes with various concentrations of ZnO nanoparticles (NPs) were characterized by scanning electron microscope (SEM), Fourier transform infrared spectroscopy (FTIR), X-ray diffraction (XRD), and membrane properties were investigated in terms of hydrophilicity, water flux, BSA solution filtration experiments, etc. Antibacterial testing was also performed to examine the practicability of the PVDF-ZnO membranes in overcoming biofouling. The results of FTIR and XRD confirmed the presence of ZnO NPs in the polymer matrix. The membrane performance demonstrated the significance of hydrophilic nanoparticles towards the enhancement of membrane properties. The optimum amount of ZnO NPs was 1.5 wt% with a lower contact angle as well as highest flux and lowest filtration resistance. The presence of ZnO NPs in the membrane matrix exhibited a strong antibacterial activity increased with the increasing ZnO NPs' content. Incorporation of ZnO NPs into PVDF membranes may have great potential in developing high-performance antifouling membranes for separation process.

Key words | antibacterial, antifouling, fouling mechanism, PVDF, ZnO nanoparticles

Juan Xiong
College of Science,
Huazhong Agricultural University,
Wuhan 430070,
China

Yexia Gong
Ningbo Institute of Innovation Research,
Ningbo FOTILE Kitchenware co., LTD,
Ningbo 315336,
China

Cong Ma (corresponding author)
State Key Laboratory of Separation Membranes and Membrane Processes, School of Environmental and Chemical Engineering,
Tianjin Polytechnic University,
Tianjin, 300387,
China
E-mail: *macong_0805@126.com*

Xingtao Zuo
Jiajie He
College of Resources and Environment,
Huazhong Agricultural University,
Wuhan 430070,
China

INTRODUCTION

Membrane filtration has been increasingly used in wastewater reuse and reclamation due to high effluent quality and reduced footprint compared with conventional processes. Among the membrane-forming materials, polyvinylidene fluoride (PVDF) has attracted considerable attention in industrial applications, mainly due to its excellent physico-chemical properties. However, fouling of PVDF membrane hinders its efficient application.

The rapid growth in nanotechnology has spurred significant interest in the environmental applications of nanomaterials. In particular, its potential to revolutionize century-old conventional water treatment processes has been enunciated. Several antimicrobial nanomaterials, such as chitosan, nAg, TiO_2, and carbon nanotubes (CNTs) show promise as alternatives to traditional chemical disinfectants that are prone to generate harmful disinfection byproducts (Li *et al.* 2008). The incorporation of nanomaterial makes the polymer membranes 'reactive' instead of a simple physical barrier, achieving multiple treatment goals in one process while minimizing fouling (Qu *et al.* 2013).

ZnO is considered to be one of the most important multifunctional semiconductors with desirable properties such as hydrophilicity, photocatalytic activities, stability, and availability. Also, ZnO nanoparticles (NPs) exhibit attractive antibacterial properties due to increased specific surface area as the reduced particle size leading to enhanced particle surface reactivity (Sirelkhatim *et al.* 2015). Recently, it has been used in inorganic particle embedded polymer

doi: 10.2166/aqua.2019.004

membranes, including polyethersulfone (PES), polysalfone (PSF), and polyethylene (PE). Nano-ZnO might potentially benefit the antifouling performance and extend the service life and application field of membranes. Moreover, nano-ZnO is 75% cheaper than TiO_2 and Al_2O_3 NPs in the Chinese market (Liang *et al.* 2012). However, to the best of our knowledge, limited studies have been reported regarding the performance of ZnO NP-embedded PVDF polymeric membranes. Liang *et al.* (2012) reported that the PVDF membranes blended with nano-ZnO particles displayed significantly anti-irreversible fouling properties. Zhang *et al.* (2014) developed a PVDF-ZnO membrane with an attempt to obtain better adsorption property based on the chemical reaction of PVDF films. However, ZnO/PVDF membrane has not been characterized to elucidate the effect of ZnO content on the PVDF fouling mechanism in detail, including antimicrobial performance.

In this work, ZnO-embedded PVDF membranes were prepared with ZnO NPs as an additive via the blending method. A set of analyses including scanning electron microscope (SEM), Fourier transform infrared (FTIR), X-ray diffraction (XRD), and contact angle measurement were carried out for the membrane characteristics. The effect of ZnO content was evaluated in terms of filterability such as modified fouling index (MFI) and anti-bacterial property. Furthermore, classic fouling models were employed to investigate the effect of ZnO NPs on the fouling mechanism of PVDF membrane.

MATERIALS AND METHODS

Materials

PVDF (FR904) (MW: 600,000) was obtained from 3F New Materials Co., Ltd, China. The size of ZnO NPs was 30 nm, used as received (Aladdin Industrial Inc., China). Polyvinylpyrrolidone (PVP), dimethylacetamide (DMAC), and bovine serum albumin (BSA) (National Chemical Reagent Co., Ltd, China) were used as obtained. All reagents were employed as received without further purification. Double distilled water was used for the preparation of all the solutions.

Membrane preparation

PVDF/ZnO membranes were prepared with different content of ZnO NPs. Viscous slurries were obtained by mixing PVDF, ZnO, and PVP in DMAC at a fixed PVDF: PVP ratio of 7:0.1 (w/w). The various ZnO contents were 0, 0.5, 0.10, 1.5, 2.0, and 3.0 wt% based on the total weight of the membrane-forming materials, respectively. The resulting mixtures were left to stand for 24 h to remove air bubbles and to obtain gels, and then cast on clean glass plates using a doctor's blade. After that, the glass plates were immersed in a coagulation water bath. The formed membranes were washed and stored in ultrapure water before use. These membranes were designated as PVDF/ZnO-X, where X is the ZnO content (%) in the membrane phase.

Membrane characterization

Membrane morphology

The morphologies of these membranes were recorded by using S4800HSD ((SU8010, HITACHI, Japan). Both the membrane upper surfaces and cross sections through the membrane were examined. Cross-sections of the prepared membranes were prepared by fracturing them in liquid nitrogen. All samples were coated with a thin conductive layer of gold/palladium prior to imaging.

Fourier transform infrared spectroscopy (FTIR) analysis

Fourier transform infrared spectroscopy (FTIR) of the composite membranes was recorded using FTIR spectrometer (Equinox 55, Bruker, Japan) in the range from 4,000 to 500 cm^{-1}.

X-ray diffraction (XRD) analysis

X-ray diffraction (XRD) study of membranes was conducted with a diffractometer (D8 Advance, Bruker, German) equipped with monochromatic Cu-kα radiation ($\lambda = 0.154$ nm) under a voltage of 40 kV and a current of 40 mA. All samples were analyzed in continuous scan mode with the 2θ ranging from 10° to 80°.

Thermogravimetric analysis (TGA)

The degradation process and the thermal stability of the membranes were investigated using thermogravimetric analysis (TGA) (NETZSCHSTA 449C, Germany) under a nitrogen atmosphere using a heating rate of 10 °C/min from 50 to 800 °C.

Hydrophilicity, porosity, and pore size measurements

The hydrophilicity of the membranes was studied by the water contact angle measurements. Contact angles were obtained using an optical tensiometer (ZSA25, Kruss, German) equipped with image processing software. The contact angle values are the average of at least five measurements.

Membrane porosity (ε) was determined via gravimetric analysis using Equation (1):

$$\varepsilon = \frac{(m_1 - m_2)/\rho_w}{(m_1 - m_2)/\rho_w + m_2/\rho_m} \quad (1)$$

where m_1 is the weight of wet membrane and m_2 is the weight of dry membrane, ρ_w and ρ_m are the densities of water and dry membrane, respectively.

The average pore size (d) of the membrane could be calculated according to the pure water flux by the Guerout–Elford–Ferry equation (Vatanpour *et al.* 2012):

$$d = \sqrt{\frac{(2.9 - 1.75\varepsilon) \times 8\mu l V_w}{\varepsilon \times A \times \Delta P \times t}} \quad (2)$$

where μ is water viscosity (8.9×10^{-4} Pa·s), l is the membrane thickness, V_w is the volume of the pure water penetrating through the membrane during experimental time interval t. The effective membrane surface area (A) and the working pressure (ΔP) in the context are 43.0×10^{-4} m^2 and 0.1 MPa, respectively.

Membrane filtration tests

The separation performance of these developed membranes was investigated in batch tests using dead-end cell under constant pressure. A nitrogen gas cylinder was used to pressurize the system to the desired operating pressure. When the applied pressure was reached, the filtrate was collected and recorded continuously at equal time intervals.

The flux (J_t) of feed solution versus time was calculated as:

$$J_t = \frac{V}{A\Delta t} \quad (3)$$

where V is the permeate volume, and Δt is the time. The corresponding filtration resistance (R_t) was determined according to Darcy's law (Bolton *et al.* 2006):

$$R_t = \frac{\Delta P}{\mu J_t} \quad (4)$$

where μ is feed water viscosity.

BSA rejection (R) was measured by the solute concentration of 1 g/L using a UV-Vis analyzer, and was calculated by Equation (5):

$$R = \left(1 - \frac{C_p}{C_f}\right) \times 100\% \quad (5)$$

where C_p and C_f are the BSA concentration of the filtrate and feed solution, respectively.

Evaluation of antimicrobial property

Antibacterial activity of the membrane was examined by the following method (Hilal *et al.* 2004; Ma *et al.* 2009). *Escherichia coli* was added to beef paste peptone liquid culture medium and activated by shaking at 37 °C for 10 h. After activation, 1 mL of bacterial solution was added into the culture medium. The prepared membranes were cut into the same size disks (diameter 3 cm) and put into the culture medium. Then, the mixture was shaken at 37 °C for 24 h. After that, 0.5 mL of bacterial liquid was absorbed in 5 mL centrifugal tubes and diluted to 10^{-6} times. The numbers of colonies on the plates were then determined by the plate count method. The same experiments were repeated three times. All the above operations were performed under sterile conditions.

Membrane fouling index

The MFI (modified fouling index) developed by Arabi & Nakhla (2010) was suggested for evaluating the fouling potential characteristics of feed water based on cake filtration model and Darcy's law. MFI is defined as the slope of the linear portion of the t/V versus V filtration curve. It can also be represented as follows:

$$\frac{t}{V} = \frac{\mu R_m}{\Delta P A} + \left[\frac{\mu \alpha C_b}{2\Delta P A^2}\right] V \quad (6)$$

where μ is the viscosity of filtrate (Pa·s), R_m is the membrane resistance, C_b is macromolecules' concentration in bulk solution (kg/m^3), and α is the specific resistance (m/kg).

Modeling for membrane fouling process

To better understand the fouling behavior of BSA, the flux decline of these membranes in the dead-end cell under constant pressure could be described by different blocking mechanisms: complete blocking, standard blocking, intermediate blocking, and cake filtration. The equations of the four classic fouling models are listed in Table 1 (Bowen *et al.* 1995).

RESULTS AND DISCUSSION

Morphology

Figure 1 shows the surface and cross-section SEM images of the membranes with different compositions. As depicted in the membrane cross section, all the prepared membranes represented a typical asymmetric and highly inhomogeneous structure. The membrane cross-sections had a dense skin layer as the selective top layer and a much thicker finger-like porous sublayer. In the presence of ZnO NPs, the finger-like structure of the sublayer became more evident and the finger-like pores were slightly wider than those of the bare PVDF membrane. The formation of larger cavities could be attributed to the higher exchange rate between solvent and non-solvent due to the hydrophilic nature of nano-sized ZnO. Nanoparticles enhanced the formation of larger macropore channels (Safarpour *et al.* 2014). It is noted that with a higher ZnO content than 1.0 wt%, ZnO NPs' aggregation was observed in the inner pores of PVDF/ZnO membranes.

The surface images of all the membranes presented a highly homogeneous pore structure. Nevertheless, the existence of ZnO NPs' aggregation was observed on the membrane surface after ZnO addition. There were increased amounts of particles displayed on the modified membrane surface with the increasing ZnO NPs dosage. This meant the nanomaterial aggregation also occurred on the membrane surface in the case of high percentage ZnO loading.

Table 1 | Equations of different fouling mechanisms for dead-end filtration

Models	Equations
Complete blocking	$J_0 - J = a^* V$
Standard blocking	$1/t + b^* = J_0/V$
Intermediate blocking	$\ln J_0 - \ln J = c^* V$
Cake filtration	$(1/J) - (1/J_0) = d^* V$

*a, b, c, and d are constants.

FTIR and XRD studies

FTIR was employed to identify the chemical structure of the PVDF/ZnO membranes with various composition ratios, and the results are shown in Figure 2.

A strong absorbance at 1,178 cm^{-1} attributed to the stretching vibration of the CF bond, and the bands at 1,404, 1,272, 1,072, 975, 877, and 839 cm^{-1} were the typical stretching vibration of CF_2 groups of β-PVDF polymorphic phase (Tseng *et al.* 2012). The relative intensity of bands of β-PVDF increased (see Supplementary Material, Figure S1), suggesting that ZnO NPs' incorporation enhanced the crystallization of the β-PVDF phase. Additionally, no new bands were observed after addition of ZnO NP to the PVDF matrix, which proved that ZnO only interacted physically with PVDF by this membrane preparation method (Zhang *et al.* 2014).

Figure 3 shows the XRD patterns of the pristine PVDF and PVDF/ZnO membranes. The 2θ values at 18.5°, 20.2°, and 26.6° corresponds to (020), (110), and (022) of PVDF. The peaks at 2θ of 31.9°, 34.3°, and 36.5° are characteristic

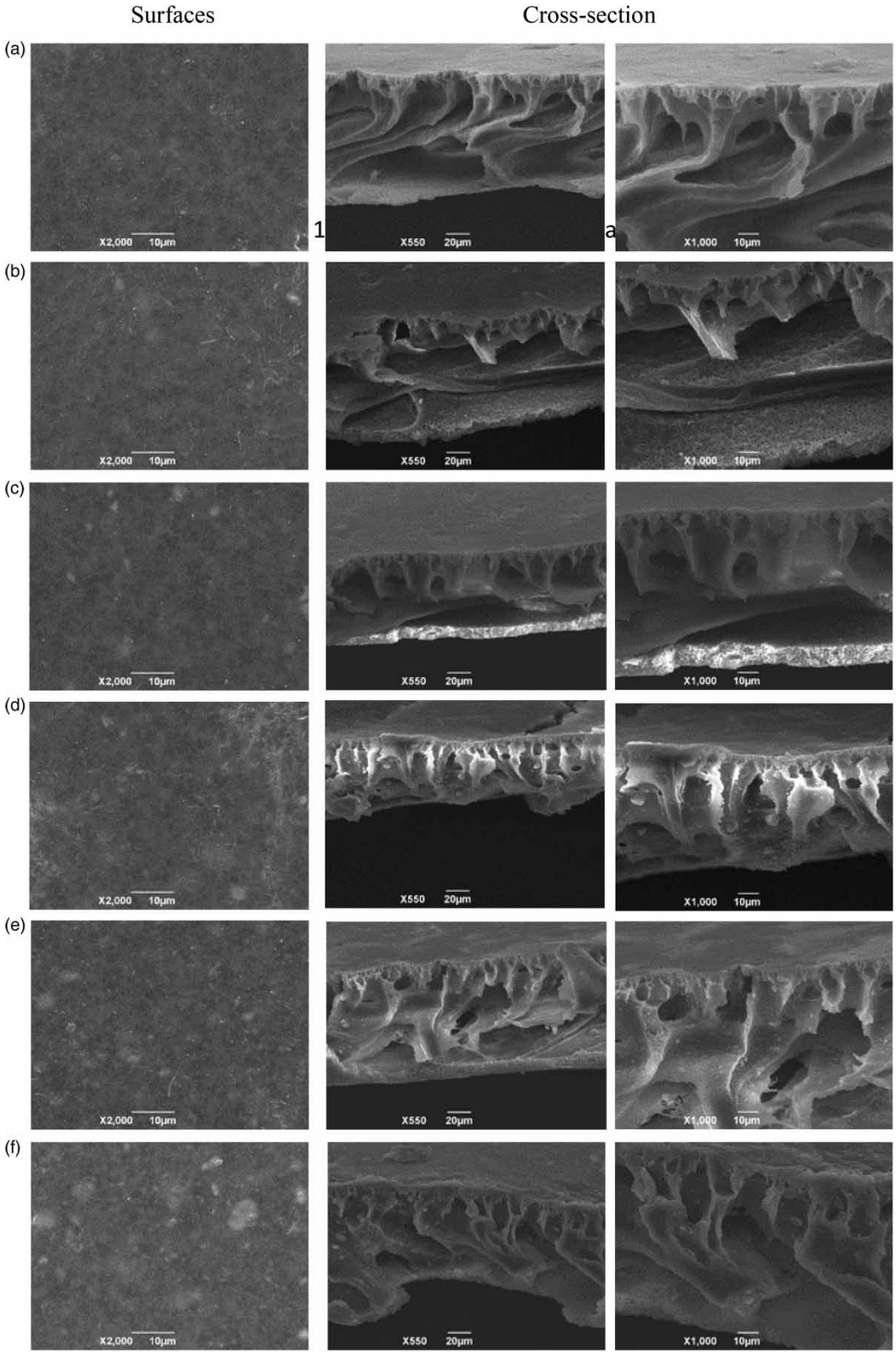

Figure 1 | SEM images of surfaces and cross sections for the PVDF/ZnO-X membranes: (a) X = 0; (b) X = 0.5; (c) X = 1.0; (d) X = 1.5; (e) X = 2.0; (f) X = 3.0.

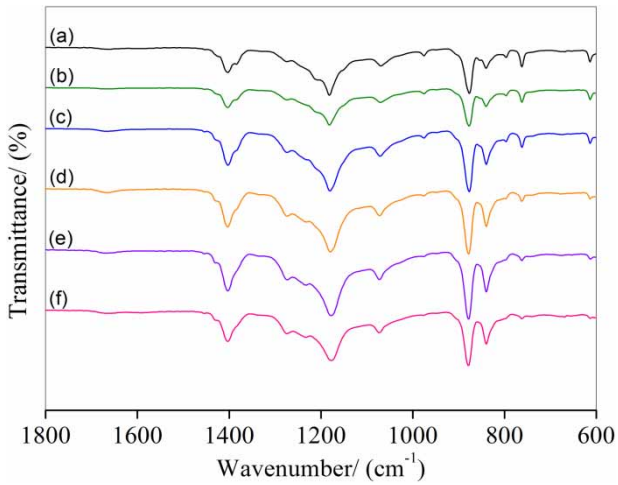

Figure 2 | FTIR spectra for the PVDF/ZnO-X membranes: (a) X = 0; (b) X = 0.5; (c) X = 1.0; (d) X = 1.5; (e) X = 2.0; (f) X = 3.0.

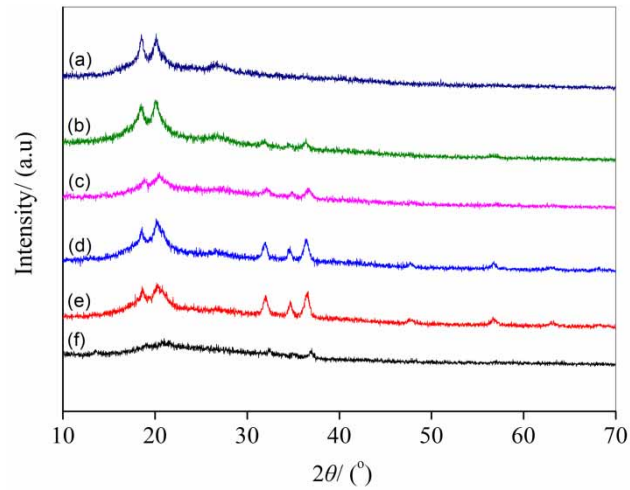

Figure 3 | XRD patterns of PVDF/ZnO-X membranes: (a) X = 0; (b) X = 0.5; (c) X = 1.0; (d) X = 1.5; (e) X = 2.0; (f) X = 3.0.

peaks of ZnO, and in agreement with the literature (Shen *et al.* 2012).

As can been seen, the diffraction curve of ZnO-embedded PVDF membrane showed the peaks at 2θ of 18.5°, 20.2°, 31.9° 34.3° and 36.5°, indicating that ZnO NPs had been distributed to the PVDF membrane matrix. Moreover, the intensities of the diffraction peaks increased to different degrees with the added ZnO NPs, which were generally related to the enhanced crystallization, formation of large crystallites, and well-ordered orientation (Cai *et al.* 2016). However, too much nano-ZnO addition restricted the cross-linking between polymers and decreased the crystallization strength as indicated in Figure 3(f).

Thermal stability (TGA analysis) studies

Thermal stability of membrane material is essential for their better application in water treatment and biotechnology. The short-term thermal stability of the prepared membranes was investigated by means of TGA and the diagrams obtained for the prepared membranes are plotted in Figure 4.

The first weight loss occurred at over 450 °C, and the polymeric matrix was further degraded, which corresponded to the decomposition of the main chains of the PVDF. It is also observed that the thermal stability of the composite material increased with the inorganic Zn content. Furthermore, all the membranes resulted in similar types of TGA curves and these membranes were kept in boiling water for a long time and no weight loss or dimensional change was observed. This study revealed that these types of organic–inorganic membranes were stable up to 250–400 °C without losing their mechanical strength and functional properties.

Membrane porosity and pore size

The porosity and pore size information of the prepared membranes are listed in Table 2. Compared with pristine PVDF membrane, the porosity of the modified membrane

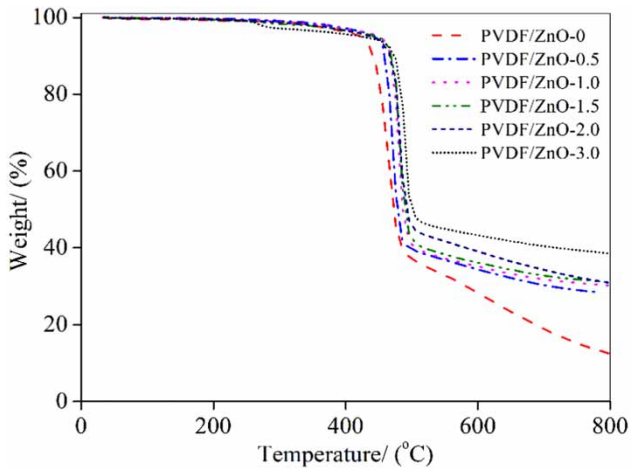

Figure 4 | TGA for neat and ZnO-embedded PVDF membrane.

Table 2 | Effect of ZnO on PVDF-ZnO membrane performance

ZnO (%)	Porosity (%)	Pore size (nm)
0.0	28.08	91.46
0.5	14.96	133.45
1.0	17.76	132.74
1.5	21.92	140.77
2.0	21.44	133.1
3.0	21.60	97.04

decreased. The result was similar to the observation of Efome *et al.* (2015), who found that the neat membrane presented the highest porosity and the minimum value was at 10 wt.% SiO_2. This is explained by: (i) the solvent competitive between the nanoparticles and porogen caused the decreased porosity of the membrane and (ii) the decrease in porosity related to the increase in viscosity caused by the increase in nanoparticle dosage (Efome *et al.* 2015). The exchange rate of the solvent and water increased due to higher concentration of hydroxyl groups, which would result in increased porosity. With the increasing ZnO NPs' content from 0.5 wt% to 1.5 wt% in the casting solution, the porosity of modified membrane increased. Further increase in the nanomaterial concentration was supposed to increase the porosity progressively but the porosities were approximately the same irrespective of concentration increase in this work. This is ascribed to the weakened effect of nanoparticles as a result of their agglomeration. Chung *et al.* (2016) have reported that the slight difference of porosity might be caused by the pores' blockage due to the high concentration of ZnO NPs.

The mean pore radius increased from 91.46 nm for pristine PVDF membrane to the maximum value of 140.77 nm for the PVDF/ZnO-1.5 membrane, followed by a decrement with the increased nanoparticles' content. ZnO incorporation decreased the interaction between the solvent and polymer, which increased the exchange rate of the solvent and nonsolvent and then caused the formation of macrovoids. However, in the case of high percentage ZnO loading, aggression was observed in the membrane cross-section as shown in Figure 1(d)–1(f), leading to membrane pores clogging (Chung *et al.* 2017). Thus, excessive nanoparticles dispersed unevenly in the casting solution, resulting in the membrane pore blockage and inducing the pore size decrease. Other research reported that the viscosity of casting solution was the major factor affecting pore size of the prepared membranes in phase inversion phenomena. High ratio addition of ZnO NPs led to an increase in viscosity which delayed the mass transfer between the solvent and non-solvent phase (Leo *et al.* 2012). Yu *et al.* (2009) reported that the formation of the nanoparticle network compressed the movement of PVDF chains, hindered the formation of macrovoid structure, and decreased the pore size. It should be noted that there was clear but no remarkable difference in mean pore size (130–140 nm) for the PVDF/ZnO membranes prepared with the ZnO concentration in the range of 0.5%–2.0%.

Pure water flux and BSA rejection

The lower contact angle represents the greater tendency for water to wet the membrane, the higher surface energy, and the higher hydrophilicity (Liu *et al.* 2012). The effect of ZnO NPs on the contact angles of the fabricated membranes with different components are shown in Figure 5. The

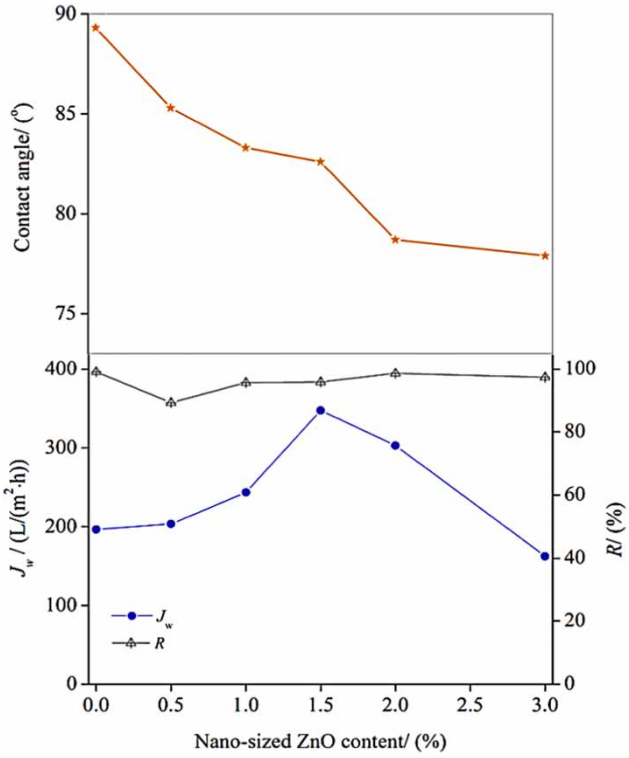

Figure 5 | Pure water fluxes and BSA rejection of the membranes.

contact angle values decreased with the increasing ZnO NPs' concentration in the membrane phase. This meant that the ZnO NPs played an important role in enhancing the surface hydrophilicity of the PVDF membranes. A similar observation has been reported by other researchers (Liang *et al.* 2012). The ZnO NPs successfully dispersed and embedded into a hydrophobic PVDF membrane phase, and it was easier for ZnO NPs on the membrane surface to form hydrogen bonds with water molecules, resulting in the increased adsorption capacity of water and improved hydrophilicity of PVDF membrane. Alhoshan *et al.* (2013) reported that incorporation of ZnO NPs changed the membrane surface density and increased the surface energy, and thus water could easily spread on the surface. The surface hydrophilicity of the membranes may affect the antifouling ability of the membranes, which is discussed in the following section.

The effect of ZnO NPs' content on pure water flux and BSA rejection of the membrane is also depicted in Figure 5. It is accepted that hydrophilicity improvement has a significant effect on the pure water flux. However, there was no consistent variation trend between flux and improved hydrophilicity as indicated in Figure 5. The water flux increased from 196.34 L/(m^2·h) for the pristine PVDF membrane to 347.55 L/(m^2·h) for the modified membrane prepared with 1.5 wt% ZnO NPs. The increased pore size and enhanced hydrophilicity were responsible for the increased permeability of pure water due to ZnO NPs in the membrane matrix, while the pure water flux decreased at ZnO content beyond 1.5%. The flux of PVDF/ZnO-3.0 membrane was lower than the pristine PVDF membrane. Liang *et al.* (2012) also reported that an over-dosage of nano-sized ZnO rendered permeability loss, and suggested that the addition of inorganic oxide to a sufficient extent could cause changes in membrane microstructure. Although no remarkable change of the porosity of the modified membranes was observed at ZnO content higher than 1.5%, the membrane permeability decreased due to the decreased pore size (Liang *et al.* 2012). Hong & He (2014) reported the decreased flux may be because the membrane pores filled due to ZnO NPs being trapped in the plyometric matrix. It is inferred that in the presence of higher ZnO NPs, pore property was the main contribution component to the permeability variation of the PVDF/ZnO membranes.

The rejection tendency of all the fabricated membranes was checked by applying BSA as organic foulant. It is clear from Figure 5 that BSA rejection decreased due to the increased pore size compared with pure PVDF membrane. Rejection increased with ZnO NPs' content from 0.5% to 2.0 wt% and was stable at 2.0% to 3.0 wt%. The result suggested that although the increased pore size was unfavorable to the BSA rejection by the membranes, the enhanced hydrophilicity of the membrane would reduce the adsorption of organic pollutants within the membrane structure (Balta *et al.* 2012). Therefore, the optimal addition of ZnO NPs in the membrane phase could maintain better BSA rejection of the prepared membrane. 1.5 wt% was a proper addition amount of ZnO NPs for the modified PVDF membrane to attain good hydrophilicity and permeability in the context. Different optimum ZnO content was obtained by Liang *et al.* (2012) in which ZnO dosage was of 1.0 wt% with a fixed PVDF:PVP ratio of 15:1 (w/w), Hong & He (2014) that ZnO dosage was of 1.5 wt% with fixed PVDF:PEG-600 ratio of 17:3 (w/w), and Zhang *et al.* (2014) that ZnO dosage was of 3.0 wt% with a fixed PVDF:PVP ratio of 14:2 (w/w), respectively.

Membrane filtration resistance

The membrane resistance is related to membrane property, and pure water was used as the feed solution. The effect of ZnO NPs' content on the membrane resistance is shown in Figure 6(a). An increased content of ZnO NPs led to decreased membrane resistance, followed by increased. PVDF/ZnO-1.5 membrane had the lowest membrane resistance. The membrane resistance for the PVDF/ZnO-3.0 membrane was higher than virgin PVDF membrane. An increased hydrophilicity improved membrane permeability, which led to the decreased membrane resistance. In addition, the membranes with larger pore sizes at the surface fouled easily (Fu *et al.* 2008). The above-mentioned behavior may be responsible for the membrane resistance variation.

The total resistance of BSA filtration versus time for the prepared membrane was also investigated and the profiles are illustrated in Figure 6(b). For the modified PVDF membranes, the total filtration resistance increased rapidly in the initial 70 min, followed by slow increase. The total

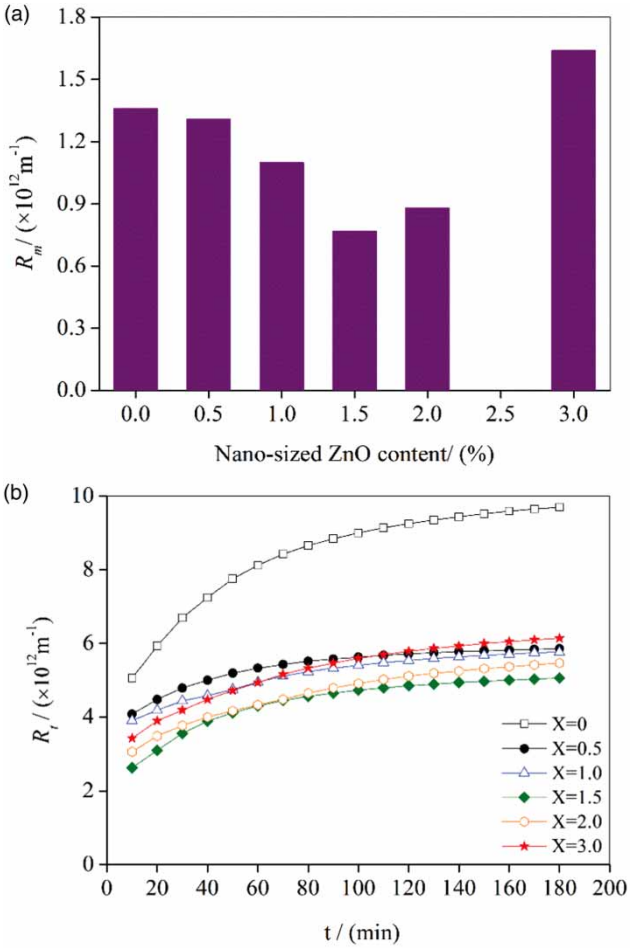

Figure 6 | Effect of nano-ZnO content on filtration resistance: (a) membrane resistance and (b) total filtration resistance of BSA.

resistance for the pristine PVDF was significantly higher than the modified membranes. PVDF/ZnO-1.5 and PVDF/ZnO-2.0 membranes exhibited a relatively lower total filtration resistance. Especially, R_t for the PVDF/ZnO-1.5 membrane had the minimal value in the filtration period, almost decreased by 48.6% compared with PVDF membrane.

The total filtration resistance was obviously higher than the membrane resistance, meaning more BSA was trapped by the membrane and then deposited on the membrane surface and pore, which caused membrane fouling and then increased the total filtration resistance. Chung *et al.* (2016) suggested that the establishment of a highly hydrophilic structure with ZnO NPs was aimed to increase the affinity of these nanoparticles to water rather than the organic matter, resulting in lower hydraulic resistance of the PVDF/ZnO membrane. Moderate addition of ZnO NPs not only reduced the membrane resistance of PVDF membrane but also the total resistance of BSA filtration.

Modified Fouling Index (MFI)

The t/V versus V filtration data were obtained for the constant pressure filtration of the BSA solution (1 g/L). MFI values of the prepared membranes are shown in Figure 7.

The pristine PVDF had a higher membrane fouling index, up to 50,574.8 s/L^2. After addition of ZnO NPs, the MFI values for the PVDF/ZnO membranes sharply decreased by 60.5%–79%. The MFI increased with the increasing ZnO NPs' concentration in the membrane phase. It was also found that MFI values for PVDF/ZnO membranes were linearly related to ZnO NPs' concentration ranging from 0.5 wt % to 3.0 wt% in the membrane matrix.

BSA is easily adsorbed on the surface of pure PVDF membrane and even enters the membrane pore, which leads to the blockage of membrane pores and causes membrane fouling. In the presence of ZnO NPs, the improved membrane hydrophilicity and permeability reduced the interaction between BSA and the membrane, which resulted in the decreased BSA adsorption and deposition on the membrane surface (Yuliwati & Ismail 2011), mitigating the formation rate of cake layers. Additionally, the increased MFI of the PVDF/ZnO membranes may be attributed to the increased total filtration resistance and membrane resistance.

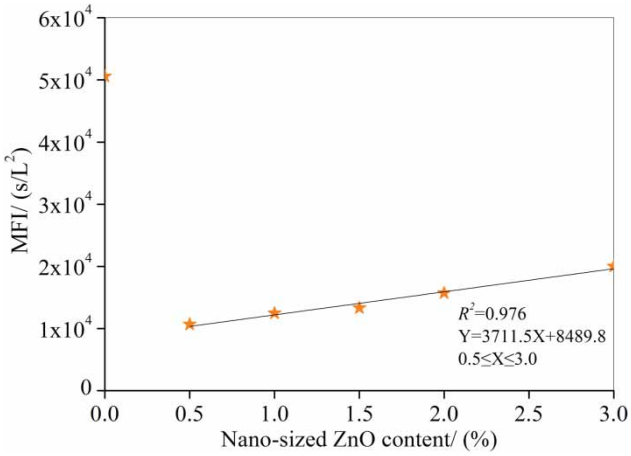

Figure 7 | Effect of ZnO content on the MFI values of the prepared membranes.

Antibacterial performance

In order to assess the antibacterial performance of the prepared membranes, Gram-negative bacteria *E. coli* was selected as the biofoulant in this work. The dilution plate method was employed to calculate the inhibition rate according to the number of viable colonies of PVDF/ZnO based on that of pristine PVDF membrane, and the results are shown in Figure S2 (Supplementary Material, Figure S2).

It is clear from Figure S2 that bacterial colonies decreased with the increasing ZnO NPs' content in the membrane phase, suggesting that the antibacterial capacity of the PVDF/ZnO membrane increased as ZnO NPs' dosage increased. The greatest antibacterial ratio was obtained for PVDF/ZnO-3.0 membrane as indicated in Table 3. This finding was in good agreement with the result of Kochkodan *et al.* (2006), who reported less adhesion of *E. coli* on the hydrophilic membrane surface. According to Li *et al.* (2008) and Sirelkhatim *et al.* (2015), the antibacterial mechanisms could be attributed to the direct contact of ZnO NPs with bacteria cell walls, resulting in bacterial cell integrity disruption.

Hence, the practicability of ZnO NPs blended PVDF membranes in bacterial growth inhibition was successfully proven with great performance. The enriched antimicrobial properties of these membranes could be further utilized in various kinds of separation and purification applications involving biofouling issues.

Table 3 | Anti-bacterial rate of PVDF/ZnO-X membrane

PVDF/ZnO-X (%)	Antibacterial rate (%)
0.5	20.97
1.0	32.26
1.5	35.48
2.0	38.71
3.0	62.90

Modeling of filtration process of BSA solution

The blocking models were applied to the constant pressure filtration of BSA solution (1 g/L) to analyze BSA fouling evolution of the prepared membranes. The permeate volume was measured as a function of time for 3 h. The permeate volume versus time data was fit using the four typical fouling models (see Supplementary Material, Figure S3). The best fouling model was selected based on the best fitted equation with the highest value of R^2 in the linear regression method. The resultant values of R^2 are presented in Table 4.

It can be seen that the standard blocking model provided the best fit of the experimental data for the fabricated membranes ($R^2 > 0.98$). The cake filtration model provided a better fit than the intermediate and complete blocking models. It is inferred that the fouling mechanism of BSA was mainly attributed to standard blocking. After addition of ZnO NPs into the PVDF membrane phase, the standard blocking model fitted very well with the experimental data. This suggested that ZnO NPs' incorporation and its concentration did not change the major membrane fouling mechanism for the BSA filtration.

CONCLUSION

PVDF-nanomaterial membranes were successfully fabricated with ZnO NPs. The hydrophilicity and permeability

Table 4 | R^2 values of the fitting four models for the prepared membranes

	R^2					
	PVDF/ZnO-X (%)					
Models	0	0.5	1.0	1.5	2.0	2.5
Complete blocking	0.711	0.721	0.850	0.670	0.862	0.831
Standard blocking	0.987	0.996	0.998	0.984	0.995	0.995
Intermediate blocking	0.783	0.762	0.882	0.746	0.914	0.884
Cake filtration	0.845	0.799	0.9098	0.812	0.952	0.926

of the blended membranes were enhanced due to the added ZnO NPs. The pore property and improved hydrophilicity decreased the PVDF/ZnO membrane filtration resistance and MFI compared with pristine PVDF membrane. The membrane containing 1.5 wt% ZnO NPs showed better separation properties. The bactericidal capacity of the prepared membranes increased with increasing ZnO NPs' concentration in the membrane matrix, thereby contributing to the reduction of membrane biofouling. Linear regression of different filtration models indicated that the main fouling mechanism of PVDF/ZnO membranes was standard blocking, which was independent of the ZnO concentration. The excellent antifouling performance, including antimicrobial property of the PVDF-ZnO membranes, is a suitable application in the membrane field.

ACKNOWLEDGEMENTS

This work was supported by the Fundamental Research Funds for the Central Universities of China (No. 2662017JC019), Hubei Provincial Natural Science Foundation of China (No. 2016CFB495), National Science Foundation of China (51508383), Natural Science Foundation of Tianjin Province (18JCQNJC09000) and the Research Fund of the Tianjin Key Laboratory of Aquatic Science and Technology (No. TJKLAST-ZD-2017-03).

SUPPLEMENTARY MATERIAL

The Supplementary Material for this paper is available online at https://dx.doi.org/10.2166/aqua.2019.004.

REFERENCES

Alhoshan, M., Alam, J., Dass, L. A. & Al-Homaidi, N. 2013 Fabrication of polysulfone/ZnO membrane: influence of ZnO nanoparticles on membrane characteristics. *Advances in Polymer Technology* **32** (4), 21369.

Arabi, S. & Nakhla, G. 2010 Impact of molecular weight distribution of soluble microbial products on fouling in membrane bioreactors. *Separation and Purification Technology* **73** (3), 391–396.

Balta, S., Sotto, A., Luis, P., Benea, L., Van der Bruggen, B. & Kim, J. 2012 A new outlook on membrane enhancement with nanoparticles: the alternative of ZnO. *Journal of Membrane Science* **389**, 155–161.

Bolton, G., LaCasse, D. & Kuriyel, R. 2006 Combined models of membrane fouling: development and application to microfiltration and ultrafiltration of biological fluids. *Journal of Membrane Science* **277** (1), 75–84.

Bowen, W. R., Calvo, J. I. & Hernández, A. 1995 Steps of membrane blocking in flux decline during protein microfiltration. *Journal of Membrane Science* **101** (1–2), 153–165.

Cai, Q., Gao, Y., Gao, T., Lan, S., Simalou, O., Zhou, X., Zhang, Y., Harnoode, C., Gao, G. & Dong, A. 2016 Insight into biological effects of zinc oxide nanoflowers on bacteria: why morphology matters. *ACS Applied Materials and Interfaces* **8** (16), 10109–10120.

Chung, Y. T., Ba-Abbad, M. M., Mohammad, A. W. & Benamor, A. 2016 Functionalization of zinc oxide (ZnO) nanoparticles and its effects on polysulfone-ZnO membranes. *Desalination and Water Treatment* **57** (17), 7801–7811.

Chung, Y. T., Mahmoudi, E., Mohammad, A. W., Benamor, A., Johnson, D. & Hilal, N. 2017 Development of polysulfone-nanohybrid membranes using ZnO-GO composite for enhanced antifouling and antibacterial control. *Desalination* **402**, 123–132.

Efome, J. E., Baghbanzadeh, M., Rana, D., Matsuura, T. & Lan, C. Q. 2015 Effects of superhydrophobic SiO_2 nanoparticles on the performance of PVDF flat sheet membranes for vacuum membrane distillation. *Desalination* **373**, 47–57.

Fu, X., Maruyama, T., Sotani, T. & Matsuyama, H. 2008 Effect of surface morphology on membrane fouling by humic acid with the use of cellulose acetate butyrate hollow fiber membranes. *Journal of Membrane Science* **320** (1–2), 483–491.

Hilal, N., Kochkodan, V., Al-Khatib, L. & Levadna, T. 2004 Surface modified polymeric membranes to reduce (bio)fouling: a microbiological study using E. coli. *Desalination* **167**, 293–300.

Hong, J. & He, Y. 2014 Polyvinylidene fluoride ultrafiltration membrane blended with nano-ZnO particle for photocatalysis self-cleaning. *Desalination* **332** (1), 67–75.

Kochkodan, V. M., Hilal, N., Goncharuk, V. V., Al-Khatib, L. & Levadna, T. I. 2006 Effect of the surface modification of polymer membranes on their microbiological fouling. *Colloid Journal* **68** (3), 267–273.

Leo, C. P., Lee, C. W. P., Ahmad, A. L. & Mohammad, A. W. 2012 Polysulfone membranes blended with ZnO nanoparticles for reducing fouling by oleic acid. *Separation and Purification Technology* **89**, 51–56.

Li, Q., Mahendra, S., Lyon, D. Y., Brunet, L., Liga, M. V., Li, D. & Alvarez, P. J. J. 2008 Antimicrobial nanomaterials for water disinfection and microbial control: potential applications and implications. *Water Research* **42** (18), 4591–4602.

Liang, S., Xiao, K., Mo, Y. & Huang, X. 2012 A novel ZnO nanoparticle blended polyvinylidene fluoride membrane for anti-irreversible fouling. *Journal of Membrane Science* **394–395**, 184–192.

Liu, Y., Yue, X., Zhang, S., Ren, J., Yang, L., Wang, Q. & Wang, G. 2012 Synthesis of sulfonated polyphenylsulfone as candidates for antifouling ultrafiltration membrane. *Separation and Purification Technology* **98**, 298–307.

Ma, N., Fan, X. F., Quan, X. & Zhang, Y. B. 2009 Ag–TiO_2/HAP/Al_2O_3 bioceramic composite membrane: fabrication, characterization and bactericidal activity. *Journal of Membrane Science* **336** (1–2), 109–117.

Qu, X., Alvarez, P. J. J. & Li, Q. 2013 Applications of nanotechnology in water and wastewater treatment. *Water Research* **47** (12), 3931–3946.

Safarpour, M., Khataee, A. & Vatanpour, V. 2014 Preparation of a novel polyvinylidene fluoride (PVDF) ultrafiltration membrane modified with reduced graphene oxide/titanium dioxide (TiO_2) nanocomposite with enhanced hydrophilicity and antifouling properties. *Industrial and Engineering Chemistry Research* **53** (34), 13370–13382.

Shen, L., Bian, X., Lu, X., Shi, L., Liu, Z., Chen, L., Hou, Z. & Fan, K. 2012 Preparation and characterization of ZnO/polyethersulfone (PES) hybrid membranes. *Desalination* **293**, 21–29.

Sirelkhatim, A., Mahmud, S., Seeni, A., Kaus, N. H. M., Ann, L. C., Bakhori, S. K. M., Hasan, H. & Mohamad, D. 2015 Review on zinc oxide nanoparticles: antibacterial activity and toxicity mechanism. *Nano-Micro Letters* **7** (3), 219–242.

Tseng, H. H., Zhuang, G. L. & Su, Y. C. 2012 The effect of blending ratio on the compatibility, morphology, thermal behavior and pure water permeation of asymmetric CAP/PVDF membranes. *Desalination* **284**, 269–278.

Vatanpour, V., Madaeni, S. S., Khataee, A. R., Salehi, E., Zinadini, S. & Monfared, H. A. 2012 TiO_2 embedded mixed matrix PES nanocomposite membranes: influence of different sizes and types of nanoparticles on antifouling and performance. *Desalination* **292**, 19–29.

Yu, L. Y., Xu, Z. L., Shen, H. M. & Yang, H. 2009 Preparation and characterization of PVDF-SiO_2 composite hollow fiber UF membrane by sol-gel method. *Journal of Membrane Science* **337** (1–2), 257–265.

Yuliwati, E. & Ismail, A. F. 2011 Effect of additives concentration on the surface properties and performance of PVDF ultrafiltration membranes for refinery produced wastewater treatment. *Desalination* **273** (1), 226–234.

Zhang, X., Wang, Y., Liu, Y., Xu, J., Han, Y. & Xu, X. 2014 Preparation, performances of PVDF/ZnO hybrid membranes and their applications in the removal of copper ions. *Applied Surface Science* **316** (1), 333–340.

First received 8 January 2019; accepted in revised form 8 October 2019. Available online 24 December 2019